HOKKAIDO UNIVERSITY

Title	Statistical properties of point vortex equilibria on the sphere
Author(s)	NEWTON, Paul; SAKAJO, Takashi
Citation	Hokkaido University Preprint Series in Mathematics, 877, 1-22
Issue Date	2007
DOI	https://doi.org/10.14943/84027
Doc URL	https://hdl.handle.net/2115/69686
Type	departmental bulletin paper
File Information	re877.pdf

Hokkaido University Collection of Scholarly and Academic Papers : HUSCAP

Statistical properties of point vortex equilibria on the sphere

P.K. NEWTON[1] T. SAKAJO[2]

[1]Department of Aerospace & Mechanical Engineering and Department of Mathematics, University of Southern California, Los Angeles, CA 90089-1191
(newton@usc.edu)

[2]Department of Mathematics, Hokkaido University
Sapporo, Japan
(sakajo@math.sci.hokudai.ac.jp)

(Received ?? and in revised form ??)

We describe a Brownian ratchet scheme which we use to calculate relative equilibrium configurations of N point vortices of mixed strength on the surface of a unit sphere. We formulate it as a linear algebra problem $A\vec{\Gamma} = 0$ where A is a $N \times N(N-1)/2$ non-normal configuration matrix obtained by requiring that all inter-vortical distances on the sphere remain constant, and $\vec{\Gamma} \in \mathbb{R}^N$ is the (unit) vector of vortex strengths which must lie in the nullspace of A. Existence of an equilibrium is expressed by the condition $\det(A^T A) = 0$, while uniqueness follows if $\mathrm{Rank}(A) = N-1$. The singular value decomposition of A is used to calculate an optimal basis set for the nullspace, yielding all values of the vortex strengths for which the configuration is an equilibrium. To home in on an equilibrium, we allow the point vortices to undergo a random walk on the sphere and after each random step we compute the smallest singular value of the configuration matrix, keeping the new arrangement only if it decreases. When the singular value drops below a predetermined convergence threshold, an equilibrium configuration is achieved and we find a basis set for the nullspace of A by calculating the right singular vectors corresponding to the singular values that are zero. For each $N = 4 \to 10$, we generate an ensemble of 1000 equilibrium configurations which we then use to calculate statistically averaged singular value distributions in order to obtain the averaged Shannon entropy and Frobenius norm of the collection. We show that the statistically averaged singular values produce an average Shannon entropy that closely follows a power-law scaling of the form $< S > \sim \alpha N^{\beta}$, where $\beta \approx 2/3$. We also show that the length of the conserved center-of-vorticity vector clusters at a value of one and the total vortex strength of the configurations cluster at the two extreme values ± 1, indicating that the ensemble average produces a single vortex of unit strength which necessarily sits at the tip of the center-of-vorticity vector. The Hamiltonian energy averages to zero reflecting a relatively uniform distribution of points around the sphere, with vortex strengths of mixed sign.

1. Introduction

We study statistical properties of collections of relative equilibrium configurations of N-point vortices on the surface of the unit sphere. The method used to produce an equilibrium is based on using the k smallest singular values of the configuration matrix (obtained by requiring that all inter-vortical distances remain fixed) as a 'ratchet', which we drive to zero by a random walk algorithm. The number of singular values that are zero correspond to the dimension of the nullspace (degree of heterogeneity) and thus the number of basis vectors needed to span the subspace of $\mathbb{R}^N$ in which the vortex strength vector lies. The decomposition method based on the nullspace of the configuration matrix was introduced in Jamaloodeen & Newton (2006) and used to determine all vortex strengths for which the Platonic solid configurations with a point vortex at each vertex form an equilibrium. Subsequently, the Brownian ratchet scheme coupled with the use of the singular value decomposition of the configuration matrix was developed by Newton & Chamoun (2007a) and used to study equilibrium configurations in the planar N-vortex problem. The singular value decomposition gives rise to the 'optimal' basis set in which to represent the vortex strength vector and also produces a characteristic 'distribution' of singular values that allows us to calculate other important quantities, such as the Shannon entropy and the size of the configuration, based on the Frobenius norm. Here, we use the method to produce an unbiased ensemble of 1000 equilibrium configurations on the unit sphere for each value of N ranging from $N = 4 - 10$ which we use to study their statistical properties. These equilibria all have configuration matrices with one-dimensional nullspaces and hence a unique vector of vortex strengths and typically, they have no discernible symmetries. Previous results on relative equilibria of point vortices on the sphere, such as that of Lim, Montaldi, and Roberts (2001) or Newton & Shokraneh (2006), assume the vortex strengths to be equal (hence without loss of generality unity), or occurring in equal and opposite pairs in the case where N is even, hence the set of equilibria was much more restrictive. By allowing the vortex strengths to take on any value, we show that the set of relative equilibrium configurations is far richer and can form the basis for a meaningful statistical study via appropriate ensemble averaging.

Statistical properties of point vortex flows have been studied before, typically with the goal of making predictions on features of two-dimensional turbulence (see, for example Kraichnan & Montgomery (1980)) based on statistically averaged properties of large collections (i.e. $N \to \infty$) of equal strength vortices, or a truncated system of Fourier modes to represent the velocity field. This approach, pioneered by Onsager (1949) and used subsequently by Joyce & Montgomery (1973), Montgomery & Joyce (1974), Pointin & Lundgren (1976), Robert (1991), Robert & Sommeria (1991), Miller, Weichman and Cross (1992), Eyink & Spohn (1993), Chavanis, Sommeria & Robert (1996), Lions & Majda (2000), Bühler (2002), and most recently by Lim et. al. (2003a,b) and Lim & Nebus (2006) for the spherical problem, seeks to identify (among other things) the partial differential equation which governs the probability distribution function associated with quantities such as the averaged vorticity or velocity fields. This mean-field equation, which is typically a nonlinear elliptic equation, can then be compared with simulations done with finite values of N, and in practice, it is often pointed out that the number of point vortices need not be so large in order for the approach to be reasonably accurate, say $N \sim 100$. However for values of N much smaller than that, a mean-field approach is certainly not useful. Nonetheless, for fixed values of $N \geqslant 4$ (the cases $N = 2, 3$ are completely understood – see Kidambi & Newton (1998), Borisov & Pavlov (1998), Borisov & Lebedev (1998), Sakajo (1999), and Newton (2001), as is the integrable case for $N = 4$ (Sakajo (2007)), if no restrictions are imposed on the vortex strengths, it is now known

that there are large numbers of distinct relative equilibria (see Newton & Chamoun (2007b) for discussions of this), and one can ask about the averaged properties of an ensemble of these equilibria for each fixed N, as well as the behavior of these averages as a function of N. Since we examine these vorticity distributions on the sphere, we expect the methods to be applicable to large scale atmospheric vortices, such as Jupiter's Great Red Spot (see Marcus (1988, 1993)), particularly when statistical conclusions are called for regarding equilibrium distributions (Miller, Weichman and Cross (1992)). A comprehensive discussion of these methods applied to geophysical flows can be found in Majda & Wang (2006). To obtain results that are meaningful, it is important that each realization of such an ensemble be generated in an unbiased way, hence the ensemble averages should represent 'typical' characteristics of each member, and thus we refer to the ensemble averaged configuration as the 'typical' equilibrium, even though it does not actually correspond exactly to any one of the individual equilibria making up the ensemble. A crucial step in such an approach is the development of an efficient and unbiased random walk scheme on the surface of a sphere which we implement using a diffusion process in the plane mapped to the sphere. Hence, in this paper our goal is to use the large families of relative equilibrium configurations of mixed strength point vortices (microscopic states) to extract macroscopic properties based on their ensemble averages.

Our paper is organized as follows. In §2 we describe the basic tool we use to construct the large families of relative equilibria on the sphere, namely the singular value decomposition of the configuration matrix associated with each equilibrium. The distribution of these singular values (properly normalized) gives rise to a scalar quantity which characterizes the equilibria — the Shannon entropy of the configuration matrix. In §3 we describe the Brownian ratchet algorithm which we use to calculate the collection of equilibria for each N. In particular, we describe our random walk algorithm on the sphere and how it is used to home in on configurations of particles that produce a configuration matrix with a non-trivial nullspace. We show examples of typical relative equilibria for $N = 4, 6, 8, 10$ along with the vortex strength vectors obtained by calculating a basis set for the nullspace of the configuration matrix. We also detail the convergence properties of the Brownian ratchet scheme. In §4 we define the ensemble averages which we use for the various quantities of interest and then we describe the statistical properties associated with the collections of equilibria. Our focus is on the ensemble averaged singular value distributions of the collection, along with the corresponding averaged Shannon entropy and Frobenius norm characterizing the 'size'. §5 contains a discussion of our key findings.

2. Decomposing the pattern

The evolution equations for N-point vortices moving on the surface of the unit sphere, written in cartesian coordinates, are given by:

$$\dot{\mathbf{x}}_\alpha = \frac{1}{4\pi} {\sum_{\beta=1}^{N}}' \Gamma_\beta \frac{\mathbf{x}_\beta \times \mathbf{x}_\alpha}{(1 - \mathbf{x}_\alpha \cdot \mathbf{x}_\beta)} \qquad (\alpha = 1, ..., N) \quad \mathbf{x}_\alpha \in \mathbb{R}^3, \quad \|\mathbf{x}_\alpha\| = 1. \tag{2.1}$$

$\mathbf{x}_\alpha$ denotes the position of the αth vortex whose strength is given by $\Gamma_\alpha \in \mathbb{R}$. The prime on the summation indicates that the singular term $\beta = \alpha$ is omitted and initially, the vortices are located at the given positions $\mathbf{x}_\alpha(0) \in \mathbb{R}^3$, $(\alpha = 1, ..., N)$. The denominator in (2.1) is the intervortical distance, $l_{\alpha\beta}$, between vortex Γ_α and Γ_β since $l_{\alpha\beta}^2 \equiv \|\mathbf{x}_\alpha - \mathbf{x}_\beta\|^2 = 2(1 - \mathbf{x}_\alpha \cdot \mathbf{x}_\beta)$. As described in Newton & Shokraneh (2006), eqns (2.1) have two conserved

quantities associated with them, the Hamiltonian energy:

$$H = -\frac{1}{4\pi}\sum_{\alpha<\beta}^{N}\Gamma_\alpha\Gamma_\beta \log\|\mathbf{x}_\alpha - \mathbf{x}_\beta\| \tag{2.2}$$

and the center-of-vorticity vector

$$\mathbf{J} = \sum_{\alpha=1}^{N}\Gamma_\alpha\mathbf{x}_\alpha = \left(\sum_{\alpha=1}^{N}\Gamma_\alpha x_\alpha, \sum_{\alpha=1}^{N}\Gamma_\alpha y_\alpha, \sum_{\alpha=1}^{N}\Gamma_\alpha z_\alpha\right) = (J_x, J_y, J_z) \tag{2.3}$$

The evolution equations for the relative distances are:

$$\pi\frac{d(l^2_{\alpha\beta})}{dt} = \sum_{\gamma=1}^{N}{}''\Gamma_\gamma\left[\frac{\mathbf{x}_\beta\cdot\mathbf{x}_\gamma\times\mathbf{x}_\alpha}{l^2_{\beta\gamma}} - \frac{\mathbf{x}_\beta\cdot\mathbf{x}_\gamma\times\mathbf{x}_\alpha}{l^2_{\alpha\gamma}}\right] = \sum_{\gamma=1}^{N}{}''\Gamma_\gamma V_{\alpha\beta\gamma}d_{\alpha\beta\gamma}, \tag{2.4}$$

where $d_{\alpha\beta\gamma} \equiv \left[\frac{1}{l^2_{\beta\gamma}} - \frac{1}{l^2_{\alpha\gamma}}\right]$. Here the $''$ means the summation excludes $\gamma = \alpha$ and $\gamma = \beta$. $V_{\alpha\beta\gamma}$ is the volume of the parallelepiped formed by the vectors $\mathbf{x}_\alpha, \mathbf{x}_\beta, \mathbf{x}_\gamma$:

$$V_{\alpha\beta\gamma} = \mathbf{x}_\alpha\cdot(\mathbf{x}_\beta\times\mathbf{x}_\gamma) \equiv \mathbf{x}_\beta\cdot(\mathbf{x}_\gamma\times\mathbf{x}_\alpha) \equiv \mathbf{x}_\gamma\cdot(\mathbf{x}_\alpha\times\mathbf{x}_\beta).$$

Notice that the sign of $V_{\alpha\beta\gamma}$ can be positive or negative depending on whether the vectors form a right- or left-handed coordinate system. The relative equations of motion yield necessary and sufficient conditions for relative equilibria,

$$\frac{dl^2_{\alpha\beta}}{dt} = 0, \quad \forall\,\alpha,\beta = 1\cdots N, \quad \alpha\neq\beta. \tag{2.5}$$

2.1. *The configuration matrix approach*

Using condition (2.5) in (2.4) gives the equation for the relative equilibria:

$$\sum_{\gamma=1}^{N}{}''\Gamma_\gamma V_{\alpha\beta\gamma}d_{\alpha\beta\gamma} = 0 \tag{2.6}$$

for each value of $\alpha,\beta = 1, ..., N$. Based on the fact that (2.6) is linear in the vortex strengths, we write it as a linear matrix system

$$A\vec{\Gamma} = 0, \tag{2.7}$$

where $\vec{\Gamma} = (\Gamma_1, \Gamma_2, ..., \Gamma_N) \in \mathbb{R}^N$ is the vector of vortex strengths, and A is the $N \times N(N-1)/2$ configuration matrix whose entries, given by the terms $V_{\alpha\beta\gamma}d_{\alpha\beta\gamma}$, encode the geometry of the configuration. Without loss of generality, we normalize the vector of vortex strengths to have unit length, hence

$$\sum_{\alpha=1}^{N}\Gamma_\alpha^2 = 1. \tag{2.8}$$

Thus, we seek configurations so that

$$\det(A^TA) = 0 \tag{2.9}$$

in which case A is rank-deficient, and has a nontrivial nullspace. We seek a basis set for this subspace of $\mathbb{R}^N$. In all cases considered in this paper, Rank(A) $= N-1$, hence the vortex strength vector is unique up to $\pm$ sign. For each equilibrium, we include in the ensemble both the case $+\vec{\Gamma}$ and $-\vec{\Gamma}$, which effectively doubles our sample size from $M = 1000$ to $M = 2000$.

2.2. *Singular value decomposition*

The optimal basis set for the nullspace of A is obtained by using the singular value decomposition of the matrix. We obtain the N singular values σ_i and corresponding left and right singular vectors $\vec{u}_i \in \mathbb{R}^{N(N-1)/2}$, $\vec{v}_i \in \mathbb{R}^N$ by solving the coupled linear system

$$A\vec{v}_i = \sigma_i \vec{u}_i; \quad A^T \vec{u}_i = \sigma_i \vec{v}_i \tag{2.10}$$

where $\sigma_{max} \equiv \sigma_1 \geqslant \sigma_2 \geqslant \cdots \geqslant \sigma_{min} \equiv \sigma_N \geqslant 0$. The left and right singular vectors are used as columns to construct the orthogonal matrices U and V:

$$U = (\vec{u}_1 \quad \vec{u}_2 \quad \cdots \quad \vec{u}_N); \quad V = (\vec{v}_1 \quad \vec{v}_2 \quad \cdots \quad \vec{v}_N), \tag{2.11}$$

which produces the singular value decomposition of A:

$$A = U\Sigma V^T = \sum_{i=1}^{N} \sigma_i \vec{u}_i \vec{v}_i^T. \tag{2.12}$$

Σ is the diagonal matrix with singular values down the diagonal, ordered from largest (top left) to smallest (bottom right):

$$\Sigma = \begin{pmatrix} \sigma_{max} & 0 & \cdots & 0 & 0 \\ 0 & \sigma_2 & \cdots & 0 & 0 \\ \vdots & \vdots & \ddots & \vdots & \vdots \\ 0 & \cdots & \cdots & \sigma_{N-1} & 0 \\ 0 & \cdots & \cdots & 0 & \sigma_{min} \\ 0 & 0 & 0 & 0 & 0 \\ \vdots & \vdots & \vdots & \vdots & \vdots \\ 0 & 0 & 0 & 0 & 0 \end{pmatrix}. \tag{2.13}$$

Equivalently, multiplying the first eqn in (2.10) by A^T, the second by A, and uncoupling the two, we obtain

$$A^T A\vec{v}_i = (\sigma_i)^2 \vec{v}_i; \quad AA^T \vec{u}_i = (\sigma_i)^2 \vec{u}_i, \tag{2.14}$$

which expresses the fact that the singular values squared are the eigenvalues of the square covariance matrices $A^T A$, AA^T. We write these eigenvalues as $\lambda_i \equiv (\sigma_i)^2$. The decomposition (2.12) expresses A as a linear superposition of the rank-one matrices $\vec{u}_i \vec{v}_i^T$, $(i = 1, ..., N)$ with weighting determined by the singular values σ_i. Its optimality is seen by the fact that the mth partial sum, defined as

$$A_m = \sum_{i=1}^{m} \sigma_i \vec{u}_i \vec{v}_i^T, \quad (m \leqslant N) \tag{2.15}$$

provides the best rank-m approximation to A, as measured by the Frobenius norm. In other words, any rank-m matrix $B \neq A_m$ has the property that $\|A - B\|_F \geqslant \|A - A_m\|_F$, where $\|\cdot\|_F$ denotes the Frobenius norm defined as $\|A\|_F = \sum_{i=1}^{N} \sigma_i$.

2.3. *Shannon entropy*

To understand how the rank-one modes are distributed, it is useful to normalize each of the eigenvalues of the covariance matrices so that they lie in the range from zero to one and can be interpreted either as probabilities, or as the percentage of energy contained

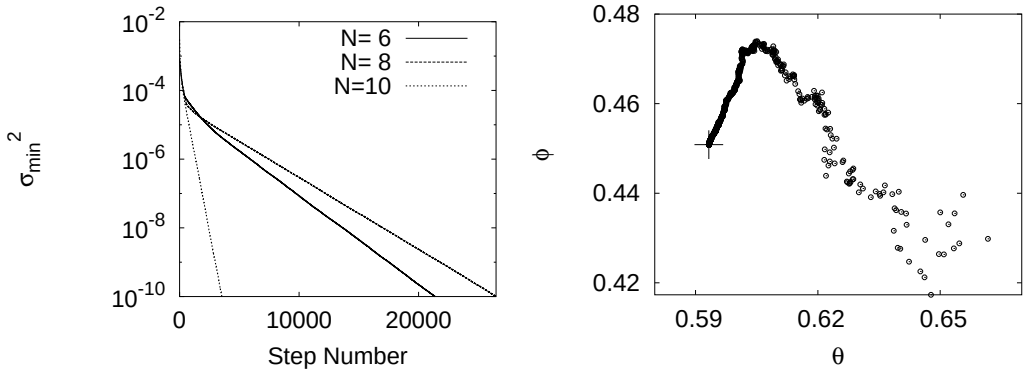

(a) (b)

FIGURE 1. (a) Convergence of the smallest singular value squared (log plot) as a function of the random walk step for $N = 6, 8, 10$; (b) Convergence of one of the point vortices making up the relative equilibrium configuration to its final position (marked '+') on the sphere.

in each mode. Hence the normalized eigenvalues are given by

$$\hat{\lambda}_i = \lambda_i / \sum_{i=1}^{k} \lambda_i. \tag{2.16}$$

The Shannon entropy, S, of the configuration matrix is obtained by using the k non-zero normalized eigenvalues $\hat{\lambda}_i$:

$$S = -\sum_{i=1}^{k} \hat{\lambda}_i \log \hat{\lambda}_i, \tag{2.17}$$

where k is the rank of A, which in this paper is $N - 1$. As discussed in Newton & Chamoun (2007b), (2.17) provides a measure of how the rank-one matrices in (2.12) are distributed in forming the configuration matrix, and thus can be thought of as a measure of 'disorder' of the pattern. In particular, if all of the weighting is in a single rank-one matrix, then A has rank-one and the Shannon entropy is minimized – its value is zero. On the other hand, if each mode has equal weighting in reconstituting the matrix, the entropy is maximum – its value is $\ln(k)$. We also note that low entropy distributions are less robust to perturbations than high entropy ones since generic perturbations will tend to *increase* the entropy of a base configuration, i.e. spread out the distribution among the modes. If the distribution is already spread out in the base state, the perturbation has a smaller effect than if the energy is clustered in one or a few modes.

3. The Brownian ratchet idea

Our method of obtaining relative equilibria is based on a Brownian 'ratchet' scheme which we implement by a diffusion process in the plane which we then map to the unit sphere. The terminology we use is borrowed from the biological literature in which molecular motors are known to extract energy from their surrounding 'heat bath' and rectify it via a ratchet mechanism. See Reimann (2002) for a comprehensive recent review. For us, the ratchet is the smallest singular value of the configuration matrix which we drive to zero. The random walk problem on the sphere is interesting in its own right, and has been studied in the past by Brillinger (1997) who considered the motion of a particle on the unit sphere heading toward a specific destination but subject to random deviations,

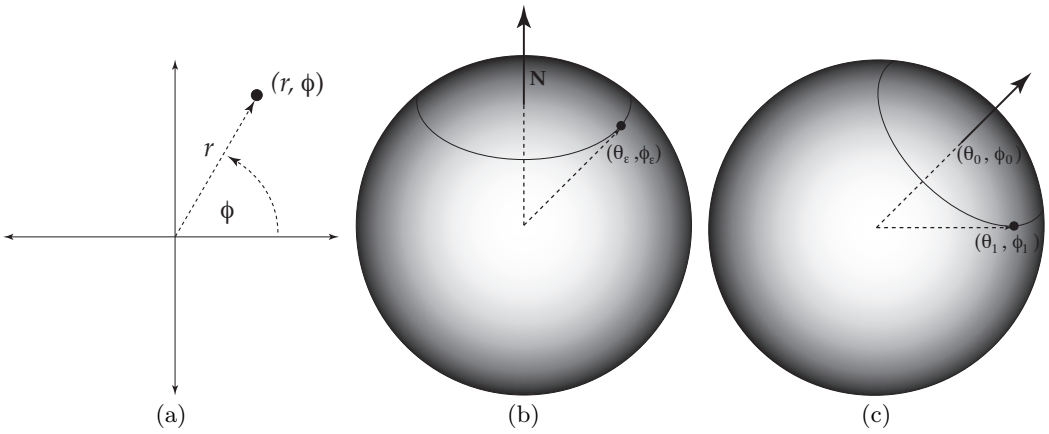

FIGURE 2. Schematic diagram depicting one random step based on an arbitrary 'seed' particle at (θ_0, ϕ_0) on the unit sphere. See text for details. (a) Step 1: A particle, initially at the origin in the plane, is diffused to a random location (r, φ) via a Gaussian process ; (b) Step 2: The point is then mapped to $(\theta_\epsilon, \phi_\epsilon)$ on the unit sphere, with the origin of the plane corresponding to the North Pole; (c) Step 3: The North Pole is rotated so that it is centered at the arbitrary 'seed' location (θ_0, ϕ_0) giving rise to the diffused point (θ_1, ϕ_1) based on that 'seed'. The process is then repeated using (θ_1, ϕ_1) as the new seed.

which he modeled as a diffusion process with drift. His motivation was to model the trajectories of certain marine mammals, and in so doing he obtained quantitative formulas for expected travel times to a spherical cap, as well as forms for limiting distributions. Indeed before this work, Kendall (1974) was interested in modeling the navigation of birds and used a pole-seeking Brownian motion model to partially explain their behavior. An early and quite general work on random walk models on the sphere and on more general Riemannian manifolds in that of Roberts & Ursell (1960).

3.1. *The ratchet scheme*

For each N, we seek configurations of particles on the unit sphere for which (2.9) is satisfied, hence $\mathrm{Rank}(A) < N$. Once such a configuration is obtained, we calculate a basis set for the nullspace of A, and hence all $\vec{\Gamma}$ satisfying (2.7) by obtaining the right singular vectors $\vec{v}_i$ defined by (2.10) corresponding to the singular values that are zero. The 'ratchet' algorithm follows the following sequence of steps:

(a) First, we distribute N points randomly on the surface of the unit sphere and calculate the configuration matrix A, finding its smallest singular value, σ_{min};

(b) We then allow each particle to execute one random step on the sphere in order to produce a new configuration matrix $\tilde{A}$, along with its smallest singular value, $\tilde{\sigma}_{min}$;

(c) If $\tilde{\sigma}_{min} \leqslant \sigma_{min}$, we keep the new configuration, otherwise we discard it;

(d) The process is repeated until $\tilde{\sigma}_{min}$ drops below a certain pre-determined threshold, which we typically choose to be $O(10^{-10})$. This 'converged' configuration is what we call a relative equilibrium;

(e) We then compute a basis set for the nullspace in order to find the corresponding vortex strengths.

Typical convergence plots are shown in figure 1. Figure 1(a) shows the decay of the smallest singular value (squared) as a function of the step number for $N = 6, 8, 10$, plotted on a log-log scale. In most cases, convergence is rapid. Figure 1(b) shows the actual path of one of the point vortices making up the configuration from its initial point to its final (converged) point (marked by a cross) on the sphere. Note that the vortex

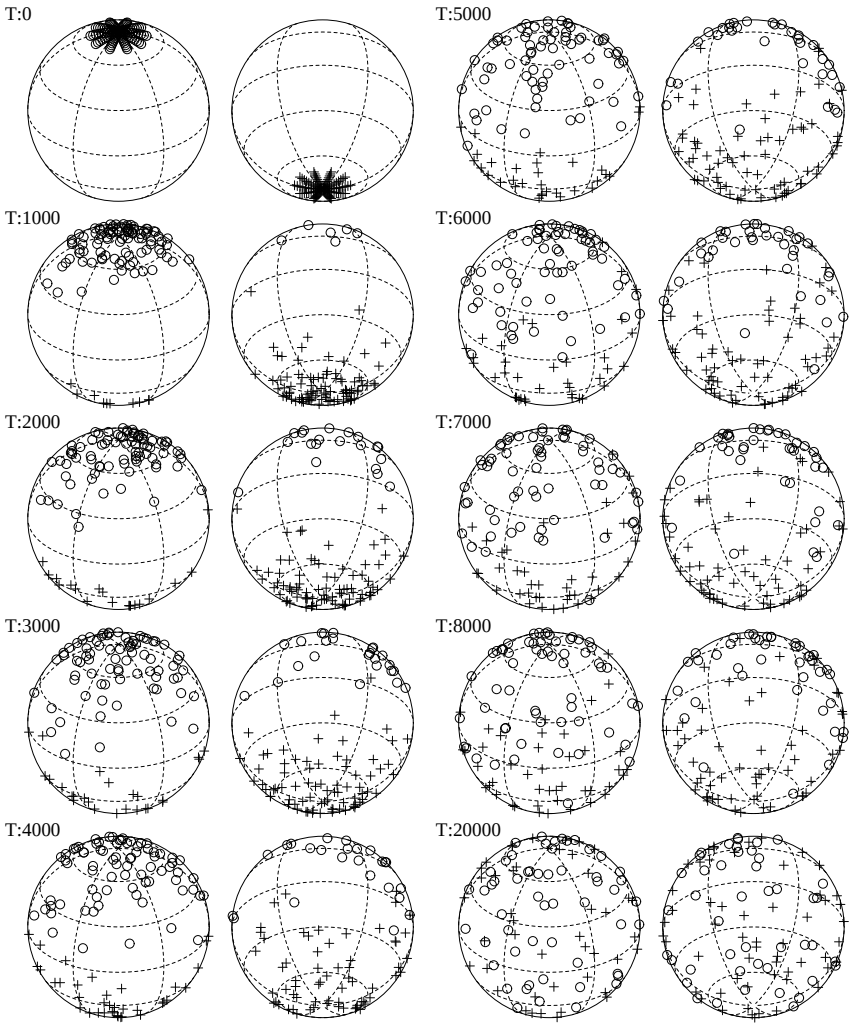

FIGURE 3. Panel depicting the random walk of collections of particles on the sphere initially clustered in spherical caps around the two poles. 'o' are clustered at the North Pole, while '+' are clustered at the South Pole. After sufficiently many steps, the particles distribute themselves about the surface of the sphere in such a way that there no longer appears to be any preference for either type of particle to be in either hemisphere. Shown are (non-dimensional) time $T = 0 - 20000$.

meanders initially before it homes in rather directly to its final location, which need not be nearby the initial location. As a general remark, we note that the singular values of a matrix are relatively insensitive to perturbations of the matrix (see Trefethen & Bau (1997)), hence we expect that the converged positions of the vortices are not far from the exact equilibrium positions when the smallest singular value is below $O(10^{-10})$.

The engine which drives the process is a random walk scheme on the sphere which we implement as follows. As shown schematically in figure 2, we start with an initial 'seed' point (θ_0, ϕ_0) on the sphere. From this point, the random walk is computed in three simple steps:

(*a*) First, we obtain a sample point in the plane from the two-dimensional Gaussian distribution, for which we compute the polar coordinate representation, (r, φ);

(*b*) Next with a scale factor ϵ (typically taken as $\epsilon = 0.01$), we rescale the point as $(\epsilon r, \varphi)$ and then map it to a corresponding point on the surface of the unit sphere centered around the North Pole so that the point is represented by $(\theta_\epsilon, \phi_\epsilon) = (\epsilon r, \varphi)$ in spherical coordinates;

(*c*) Finally, we rotate the point so that the North Pole maps to the original point (θ_0, ϕ_0), while $(\theta_\epsilon, \phi_\epsilon)$ maps to the new 'diffused' point (θ_1, ϕ_1).

The process is then iterated to obtain each subsequent point $(\theta_{n+1}, \phi_{n+1})$ starting with (θ_n, ϕ_n) as a 'seed'. Here, the procedure is implemented for a collection of particles initially clustered around the North Pole (those marked 'o'), and South Pole (those marked '+'), shown in figure 3. As the particles evolve, they gradually diffuse over the surface of the sphere, eventually giving equal probability of finding a 'o' particle or a '+' particle in any fixed two-dimensional spherical sector.

3.2. *Relative equilibria*

Typical examples of relative equilibria found this way are shown in the panels of figure 4 for $N = 4$, figure 5 for $N = 6$, figure 6 for $N = 8$, figure 7 for $N = 10$. In each figure, we present a panel of ten distinct relative equilibrium configurations showing both the vortex positions in the Northern and Southern hemispheres as well as the corresponding vector of vortex strengths $\vec{\Gamma}$. In each case, the intersection of the center-of-vorticity vector, $\mathbf{J}$ (as defined in (2.3)) with the unit sphere is marked with an 'X'. All of the cases treated in this paper have one-dimensional nullspaces, hence unique vortex strength vectors which we normalize to unity. Note that all of the configurations are manifestly asymmetric, a topic discussed in Newton & Chamoun (2007b). Examples of asymmetric equilibria are indeed rare, the first discussion of this can be found in Aref & Vainchtein (1998).

In figure 8 we show histograms of the length of the $\mathbf{J}$ vector for the cases $N = 4, 6, 8, 10$. In all cases, the peak is near the unit value, indicating that most of the states making up the ensemble can be described as not too different from single dominant vortex of near unit strength resting near the tip of the center-of-vorticity vector, with the remaining $N - 1$ weaker vortices distributed asymmetrically around the surface of the sphere. In all cases, the N vortices have mixed signs and the spread around the most likely state tightens as N increases, indicating that the limiting configuration (constrained to have Rank $= N-1$) is a single vortex of unit strength resting at the tip of the center-of-vorticity vector.

Likewise, histograms of the Hamiltonian energy (2.2) are shown in figure 9, and in each case the peak value is zero with a spread that tightens with increasing N. This limiting configuration suggests a relatively uniform distribution of points around the sphere with vortex strengths of mixed sign.

4. Statistical properties

4.1. *Ensemble averages*

The statistical properties of relative equilibria are studied by obtaining ensemble averages of collections of equilibrium configurations. For each value of $N = 4 \to 10$, we generate an ensemble of equilibrium configuration matrices, denoting each member of the ensemble $A^{(j)}$, with corresponding right nullvector $\vec{\Gamma}^{(j)}$. The initial sample size for each case is nominally $M = 1000$ which we double to $M = 2000$ by including both $\pm\vec{\Gamma}^{(j)}$. The singular values for the jth realization are denoted by $\sigma^{(j)}_{max} \equiv \sigma^{(j)}_1 \geqslant \sigma^{(j)}_2 \geqslant ... \geqslant \sigma^{(j)}_{min} \equiv$

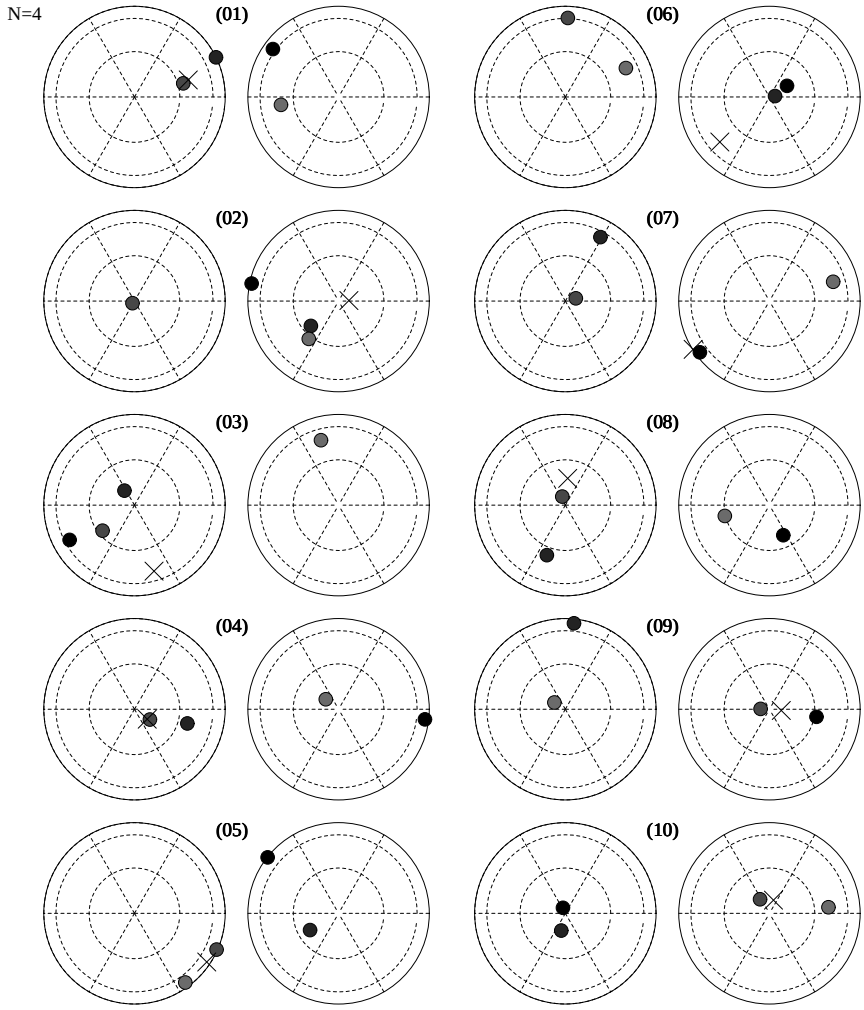

FIGURE 4. $N = 4$: Panel of ten different converged equilibrium configurations each with one-dimensional nullspaces. Shown are the Northern and Southern hemisphere projections, with 'X' marking the intersection of $\mathbf{J}$ with the unit sphere. Starting at the top left and proceeding down the left column, the vortex strengths are given by $(8.22e-02, 9.32e-02, -5.26e-01, 8.41e-01)$; $(-9.54e-02, 1.27e-02, -9.67e-03, -9.95e-01)$; $(-2.73e-02, -2.87e-02, -9.99e-01, 1.42e-02)$; $(-6.03e-04, -5.01e-03, -9.97e-01, 7.46e-02)$; $(-9.69e-01, -2.29e-01, 4.99e-02, 7.54e-02)$; $(-1.60e-01, 1.75e-01, -9.19e-01, -3.14e-01)$; $(9.51e-01, 6.15e-03, -3.07e-01, -2.90e-02)$; $(-5.04e-01, -2.23e-01, -1.89e-01, 8.13e-01)$; $(9.24e-02, 6.72e-02, -9.80e-01, 1.64e-01)$; $(-1.79e-02, -8.13e-02, 2.33e-01, 9.69e-01)$.

$\sigma_N^{(j)} \geqslant 0$ and their corresponding left and right singular vectors are denoted by $\vec{u}_i^{(j)}$ and $\vec{v}_i^{(j)}$ $(i = 1, ..., N)$ respectively. We define the ensemble average of the collection of configuration matrices

$$< A >_M = \frac{1}{M} \sum_{j=1}^{M} A^{(j)}; \quad < A >_\infty = \lim_{M \to \infty} < A >_M \tag{4.1}$$

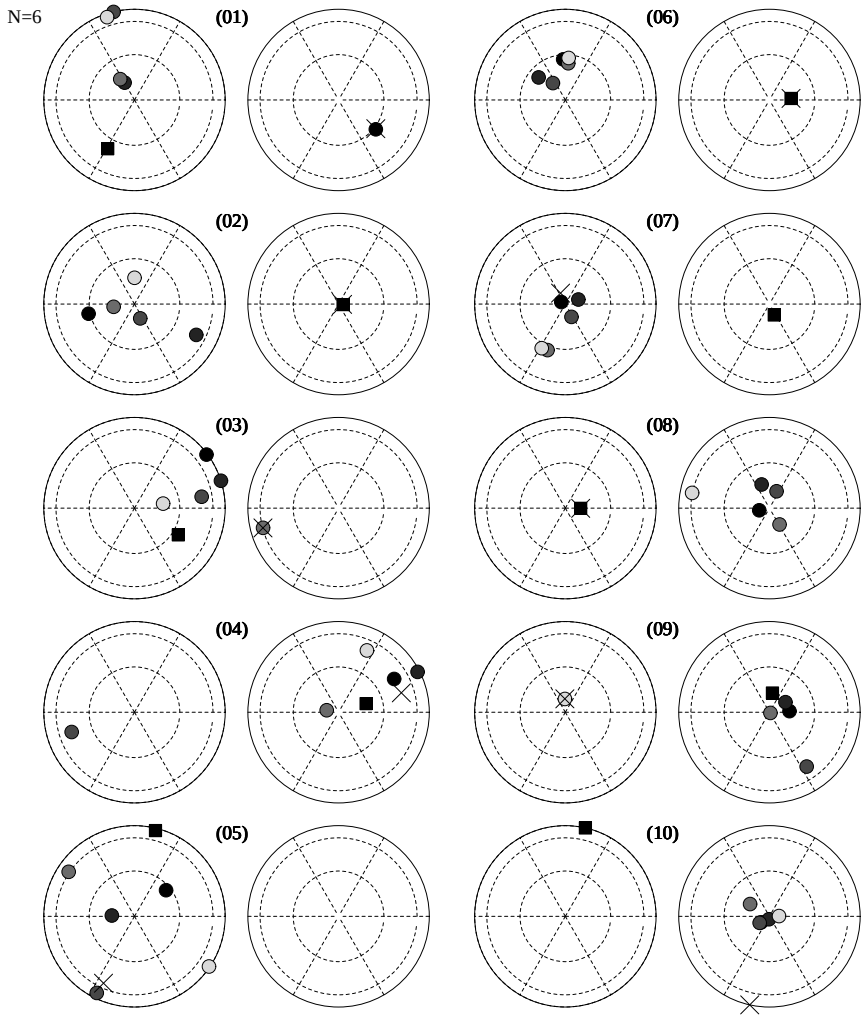

FIGURE 5. $N = 6$: Panel of ten different converged equilibrium configurations each with one-dimensional nullspaces. Shown are the Northern and Southern hemisphere projections, with 'X' marking the intersection of **J** with the unit sphere. Starting at the top left and proceeding down the left column, the vortex strengths are given by $(9.99e-01, 1.21e-03, -1.33e-03, 8.55e-04, 6.86e-03, -1.87e-03)$; $(-1.54e-03, -9.28e-03, -4.92e-03, -2.30e-03, -4.36e-03, 9.99e-01)$; $(1.15e-03, 2.46e-03, 9.98e-01, 4.47e-02, -4.36e-03, -3.73e-03)$; $(1.24e-02, -1.51e-02, 8.53e-05, -9.99e-01, -5.77e-03, -1.20e-02)$; $(2.51e-01, 5.25e-03, 2.65e-01, 8.99e-01, 1.73e-01, -1.71e-01)$; $(2.35e-04, 1.03e-05, 3.80e-04, -1.39e-04, -4.22e-04, 9.99e-01)$; $(1.38e-03, 3.32e-04, 1.68e-05, -7.09e-04, -1.83e-05, -9.99e-01)$; $(-5.01e-03, -3.10e-04, 7.89e-04, 4.57e-04, -2.88e-04, 9.99e-01)$; $(2.47e-04, -4.90e-06, -1.92e-03, -2.18e-03, 9.99e-01, 6.28e-04)$; $(-1.45e-03, 6.92e-03, -1.94e-02, 1.65e-03, -8.50e-03) - 9.99e-01)$;.

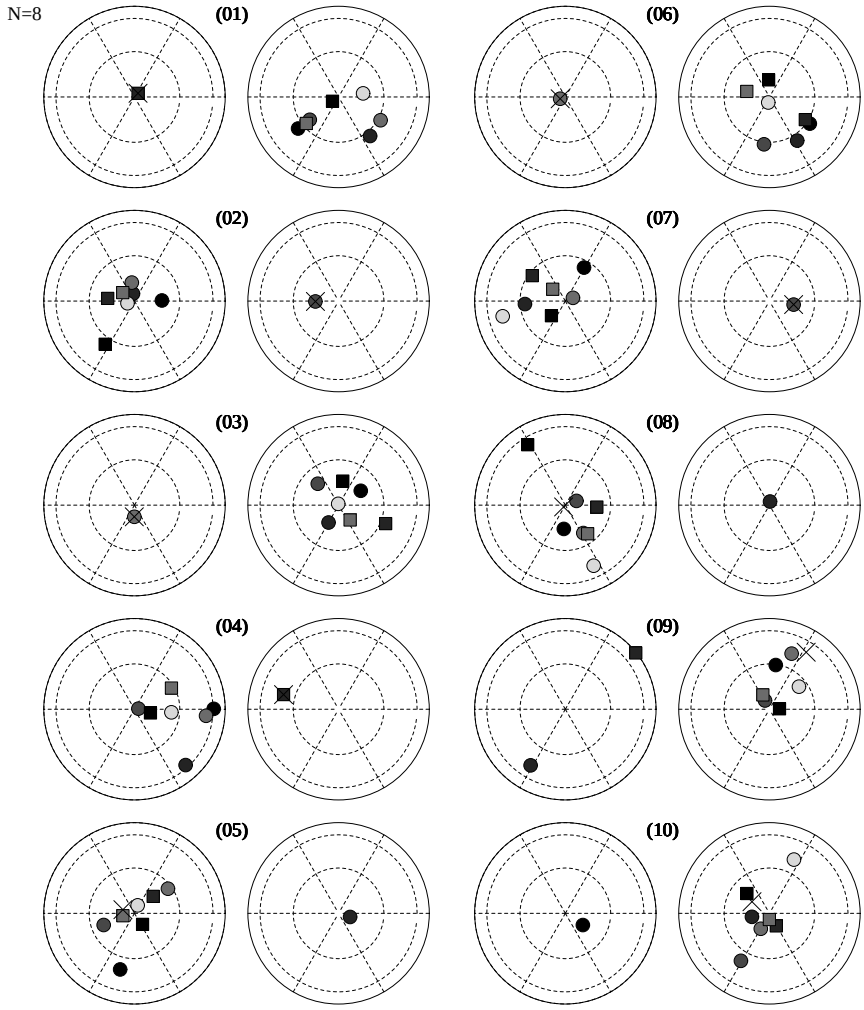

FIGURE 6. $N = 8$: Panel of ten different converged equilibrium configurations each with one-dimensional nullspaces. Shown are the Northern and Southern hemisphere projections, with 'X' marking the intersection of **J** with the unit sphere. Starting at the top left and proceeding down the left column, the vortex strengths are given by $(1.23e-04, -6.62e-05, 3.76e-05, 1.01e-05, -2.96e-04, -2.80e-03, 9.99e-01, -7.44e-05)$; $(-8.70e-03, 1.15e-03, -1.00e-03, 9.99e-01, -8.58e-04, -1.28e-03, 5.99e-04, -8.68e-04)$; $(1.61e-03, 8.76e-04, 9.99e-01, 1.88e-03, -2.67e-03, -8.81e-04, -5.10e-04, 8.66e-04)$; $(6.41e-04, 6.88e-04, -4.76e-04, -2.49e-04, -9.15e-04, 9.97e-04, 9.99e-01, 6.67e-04)$; $(-1.02e-03, -9.99e-01, -1.72e-03, -5.12e-04, -3.59e-04, -3.65e-04, 1.51e-03, 2.31e-03)$; $(2.58e-04, -5.37e-05, 9.99e-01, 2.90e-04, -1.40e-03, -6.43e-04, -1.69e-04, 5.52e-04)$; $(9.13e-04, -1.53e-03, 9.73e-05, 9.99e-01, 1.11e-03, 9.08e-05, 2.80e-04, -1.53e-03)$; $(7.74e-03, -9.99e-01, -6.24e-04, -8.47e-04, 2.83e-03, 3.64e-02, 3.83e-03, 1.03e-03)$; $(4.03e-03, -9.99e-01, 1.17e-03, 1.17e-04, 9.41e-04, -7.53e-05, 4.45e-02, -1.00e-04)$; $(-9.99e-01, 9.12e-04, -4.47e-04, 1.26e-03, 1.33e-03, 1.47e-03, -1.69e-04, 6.57e-04)$;.

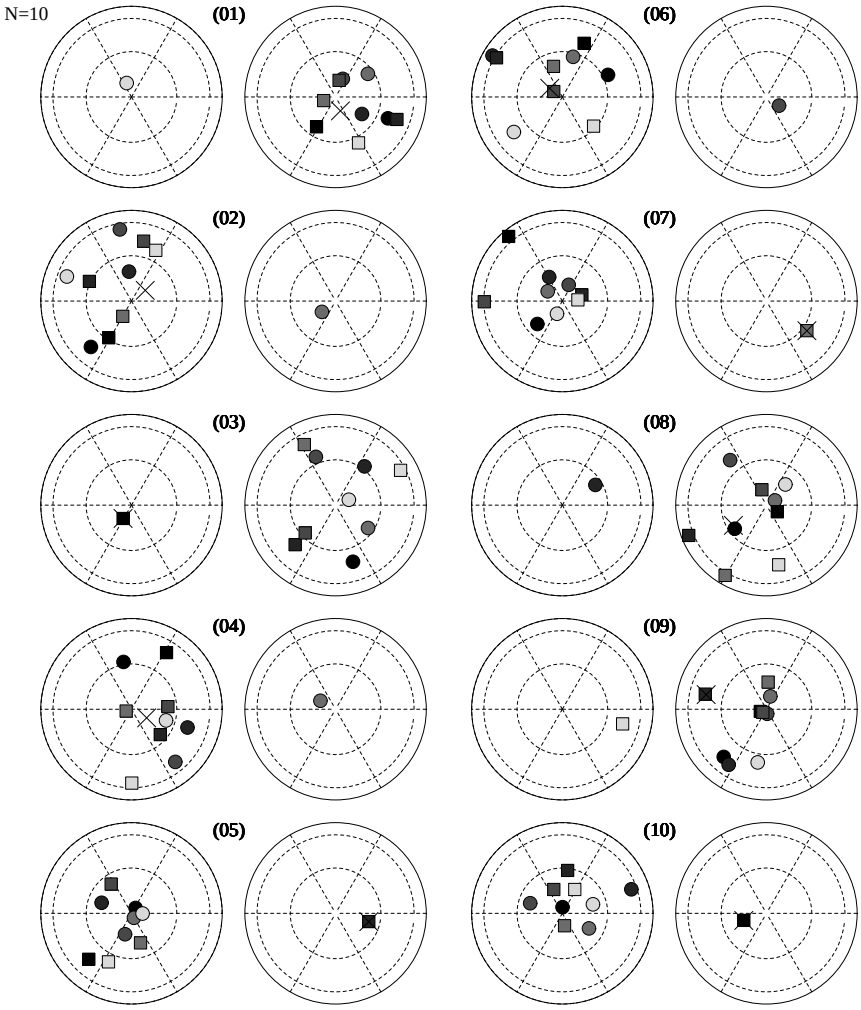

FIGURE 7. $N = 10$: Panel of ten different converged equilibrium configurations each with one-dimensional nullspaces. Shown are the Northern and Southern hemisphere projections, with 'X' marking the intersection of **J** with the unit sphere. Starting at the top left and proceeding down the left column, the vortex strengths are given by
$(-1.60e{-}03, 1.31e{-}03, 1.88e{-}03, -1.61e{-}04, -9.99e{-}01, 8.35e{-}04, 8.05e{-}04, 1.00e{-}03, 2.34e{-}04, 1.38e{-}03)$;
$(1.47e{-}03, 8.97e{-}03, -9.99e{-}01, -1.85e{-}03, 4.53e{-}04, -3.37e{-}03, -6.19e{-}03, 6.59e{-}03, -1.02e{-}03, 6.36e{-}05)$;
$(2.46e{-}04, -1.72e{-}04, 2.20e{-}03, -8.13e{-}04, -7.56e{-}03, 9.99e{-}01, 1.46e{-}03, 2.44e{-}03, 7.21e{-}04, 2.39e{-}03)$;
$(6.20e{-}04, 5.14e{-}03, -9.99e{-}01, -8.33e{-}04, -2.21e{-}03, 2.56e{-}03, 4.37e{-}04, 1.33e{-}02, 4.04e{-}03, 5.59e{-}03)$;
$(-3.91e{-}05, -1.79e{-}03, -4.78e{-}04, 4.96e{-}05, 4.45e{-}04, 4.08e{-}04, 9.99e{-}01, 8.77e{-}04, 4.37e{-}04, -2.23e{-}04)$;
$(1.37e{-}04, 1.36e{-}03, -1.54e{-}05, -9.99e{-}01, -7.70e{-}04, -1.38e{-}03, -2.72e{-}03, 1.17e{-}04, 1.96e{-}03, -2.31e{-}03)$;
$(7.99e{-}04, -8.61e{-}04, -2.12e{-}04, 1.82e{-}03, -2.67e{-}04, 8.14e{-}04, -3.05e{-}04, 9.99e{-}01, 9.86e{-}05, 1.51e{-}04)$;
$(9.95e{-}03, -9.99e{-}01, 1.30e{-}05, -1.15e{-}03, -6.55e{-}04, -1.08e{-}04, -1.83e{-}03, -2.54e{-}04, 9.63e{-}05, -2.73e{-}03)$;
$(4.22e{-}04, 1.91e{-}04, -4.14e{-}04, 8.39e{-}04, -1.05e{-}04, 4.51e{-}04, 4.68e{-}02, 8.80e{-}04, -1.76e{-}04, -9.98e{-}01)$;
$(-4.09e{-}04, -2.58e{-}03, -1.20e{-}03, -5.46e{-}04, -9.31e{-}04, 9.99e{-}01, -1.26e{-}04, -6.47e{-}04, -1.64e{-}05, -1.19e{-}03)$;.

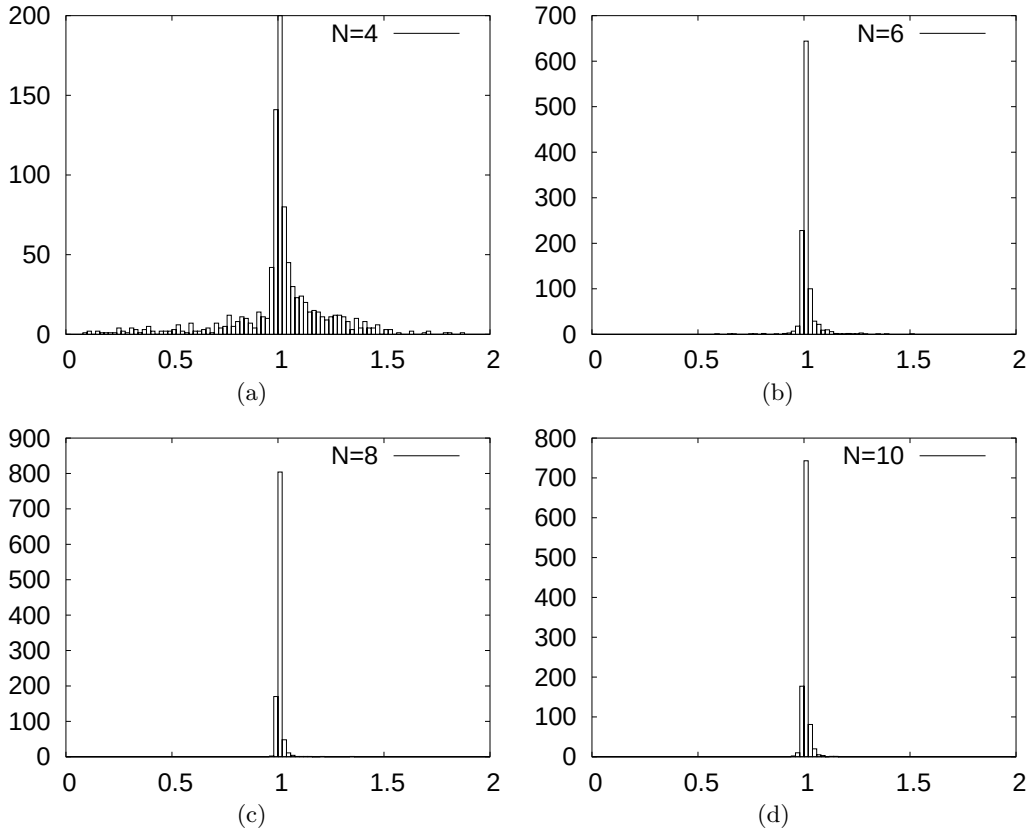

FIGURE 8. Histograms of the length of the center-of-vorticity vector $\|\mathbf{J}\|$. In each case, the peak clusters around the unit value which would be its value if there was a single point vortex of unit strength.

as well as the ensemble averages of the singular components:

$$< \sigma_i >_M = \frac{1}{M}\sum_{j=1}^{M} \sigma_i^{(j)}; \quad < \sigma_i >_\infty = \lim_{M\to\infty} < \sigma_i >_M, \tag{4.2}$$

$$< \lambda_i >_M = \frac{1}{M}\sum_{j=1}^{M} \lambda_i^{(j)}; \quad < \lambda_i >_\infty = \lim_{M\to\infty} < \lambda_i >_M \tag{4.3}$$

The standard deviation of each quantity is denoted with double brackets $<< \cdot >>$. We denote the averaged normalized values

$$< \hat{\sigma}_i >_M = \frac{1}{M}\sum_{j=1}^{M} \hat{\sigma}_i^{(j)}; \quad < \hat{\sigma}_i >_\infty = \lim_{M\to\infty} < \hat{\sigma}_i >_M, \tag{4.4}$$

$$< \hat{\lambda}_i >_M = \frac{1}{M}\sum_{j=1}^{M} \hat{\lambda}_i^{(j)}; \quad < \hat{\lambda}_i >_\infty = \lim_{M\to\infty} < \hat{\lambda}_i >_M \tag{4.5}$$

with standard deviations $<< \hat{\cdot} >>$. We then define the Shannon entropy of the jth member of the ensemble to be

$$S^{(j)} = -\sum_{i=1}^{k} \hat{\lambda}_i^{(j)} \log \hat{\lambda}_i^{(j)}, \tag{4.6}$$

with ensemble average

$$< S >_M = \frac{1}{M}\sum_{j=1}^{M} S^{(j)}; \quad < S >_\infty = \lim_{M\to\infty} < S >_M, \tag{4.7}$$

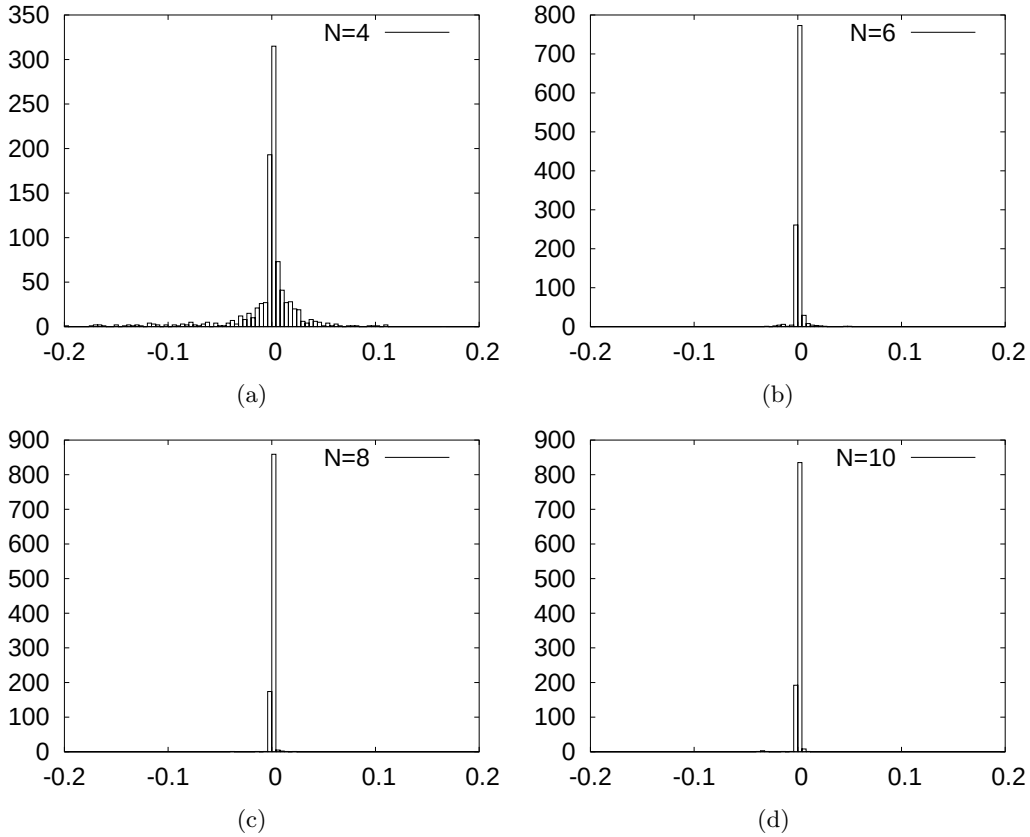

FIGURE 9. Histograms of the Hamiltonian energy H. In each case, the peak clusters around zero, indicating a relatively even distribution of points around the sphere with vortex strengths of mixed sign.

and standard deviation $<< S >>$.

4.2. *Statistical properties*

Here we summarize the main results based on an analysis of the ensemble averages for the cases $N = 4, 5, 6, 7, 8, 9, 10$. Table 1 shows the ensemble averaged properties of the singular values, listed in decreasing order, for the case $N = 10$. For each of the ten singular values, we show the maximum value in the ensemble ($max_j \sigma_i^{(j)}$), the minimum value ($min_j \sigma_i^{(j)}$), the sample mean ($< \sigma_i >_M$), and the sample standard deviation ($<< \sigma_i >>_M$) for $M = 1000$. The smallest singular value, σ_{10}, has converged to the sample average $< \sigma_{10} >_{1000} = 9.97 \times 10^{-11}$. In Table 2 we show the corresponding results for the normalized family of singular values $\hat{\sigma}_i$. Here, the smallest sample average is $< \hat{\sigma}_{10} >_{1000} = 5.09 \times 10^{-12}$ with a gap of ten orders of magnitude between it and the next smallest value $< \hat{\sigma}_9 >_{1000} = 1.39 \times 10^{-2}$. The size of the smallest singular value, the gap between it and the next smallest, and the steady decrease of the convergence curve shown in figure 1(a) gives us confidence that we are in close proximity to an equilibrium configuration. Figure 10 shows the distribution of the normalized singular values for $N = 4, 6, 8, 10$. A noteworthy feature is that the shape of the distribution for the final two cases $N = 8, 10$ is quite similar, indicating convergence to a fixed distribution as a function of N.

Sing vals	$max_j \sigma_i^{(j)}$	$min_j \sigma_i^{(j)}$	$< \sigma_i >_M$	$<< \sigma_i >>_M$
σ_1	3.72e+02	1.88e+00	8.73e+00	2.00e+01
σ_2	3.71e+02	1.75e+00	8.43e+00	2.01e+01
σ_3	4.77e+01	1.22e+00	3.18e+00	2.28e+00
σ_4	4.22e+01	8.99e-01	2.59e+00	1.98e+00
σ_5	1.16e+01	7.06e-01	1.70e+00	7.40e-01
σ_6	4.93e+00	4.61e-01	1.24e+00	5.08e-01
σ_7	3.81e+00	2.73e-01	8.44e-01	3.21e-01
σ_8	2.56e+00	9.92e-02	5.36e-01	2.27e-01
σ_9	1.03e+00	7.44e-03	2.75e-01	1.36e-01
σ_{10}	9.99e-11	9.54e-11	9.97e-11	4.07e-13

TABLE 1. Maximum value, minimum value, sample mean and standard deviation for the $N = 10$ ensemble averaged singular values (not normalized) based on a sample size of $M = 1000$.

Sing vals	$max_j \hat{\sigma}_i^{(j)}$	$min_j \hat{\sigma}_i^{(j)}$	$< \hat{\sigma}_i >_M$	$<< \hat{\sigma}_i >>_M$
$\hat{\sigma}_1$	4.95e-01	1.72e-01	2.74e-01	5.76e-02
$\hat{\sigma}_2$	4.95e-01	1.51e-01	2.56e-01	6.20e-02
$\hat{\sigma}_3$	2.60e-01	2.21e-03	1.38e-01	3.64e-02
$\hat{\sigma}_4$	2.15e-01	2.11e-03	1.12e-01	3.26e-02
$\hat{\sigma}_5$	1.38e-01	1.98e-03	7.84e-02	2.48e-02
$\hat{\sigma}_6$	1.14e-01	1.53e-03	5.78e-02	1.99e-02
$\hat{\sigma}_7$	8.74e-02	9.52e-04	4.06e-02	1.58e-02
$\hat{\sigma}_8$	7.60e-02	8.96e-04	2.62e-02	1.21e-02
$\hat{\sigma}_9$	4.65e-02	2.31e-04	1.39e-02	8.21e-03
$\hat{\sigma}_{10}$	1.10e-11	1.19e-13	5.09e-12	2.03e-12

TABLE 2. Maximum value, minimum value, sample mean and standard deviation for the $N = 10$ ensemble averaged singular values (normalized) based on a sample size of $M = 1000$.

In Table 3 we show the statistical properties of the averaged Shannon entropy and Frobenius norms for $N = 4, 5, 6, 7, 8, 9, 10$. These quantities, shown as a function of the sample size M are depicted in figures 11 and 13. It is interesting to note from figure 11, the spacing of the converged values is quite regular, indicating an underlying scaling law. Indeed, in figure 12 we show the ensemble averaged Shannon entropy values shown in Table 3 plotted as a function of N on a log-log scale. The data shows power-law scaling of the form $< S > \sim \alpha N^{\beta}$, with $\alpha \sim 0.305683$, $\beta \sim 0.671424$ as obtained via a least squares fit to the data. In figure 14 we show histograms of the total vortex strength of each equilibrium. We note the tendency for $\sum_{i=1}^{N} \Gamma_i$ to cluster at the extreme values ± 1 in agreement with the observation that the histograms of $\|\mathbf{J}\|$ in figure 8 cluster around one. The 'pure translation' case $\sum_{i=1}^{N} \Gamma_i = 0$ appears to be quite rare although there are examples of pure translational equilibria in the samples.

5. Discussion

The richness of the class of relative equilibria provided by solving the linear algebra problem (2.7) for each N allowed us to use them as microstates from which to extract information on the macroscopic level via ensemble averages. There are two main findings:

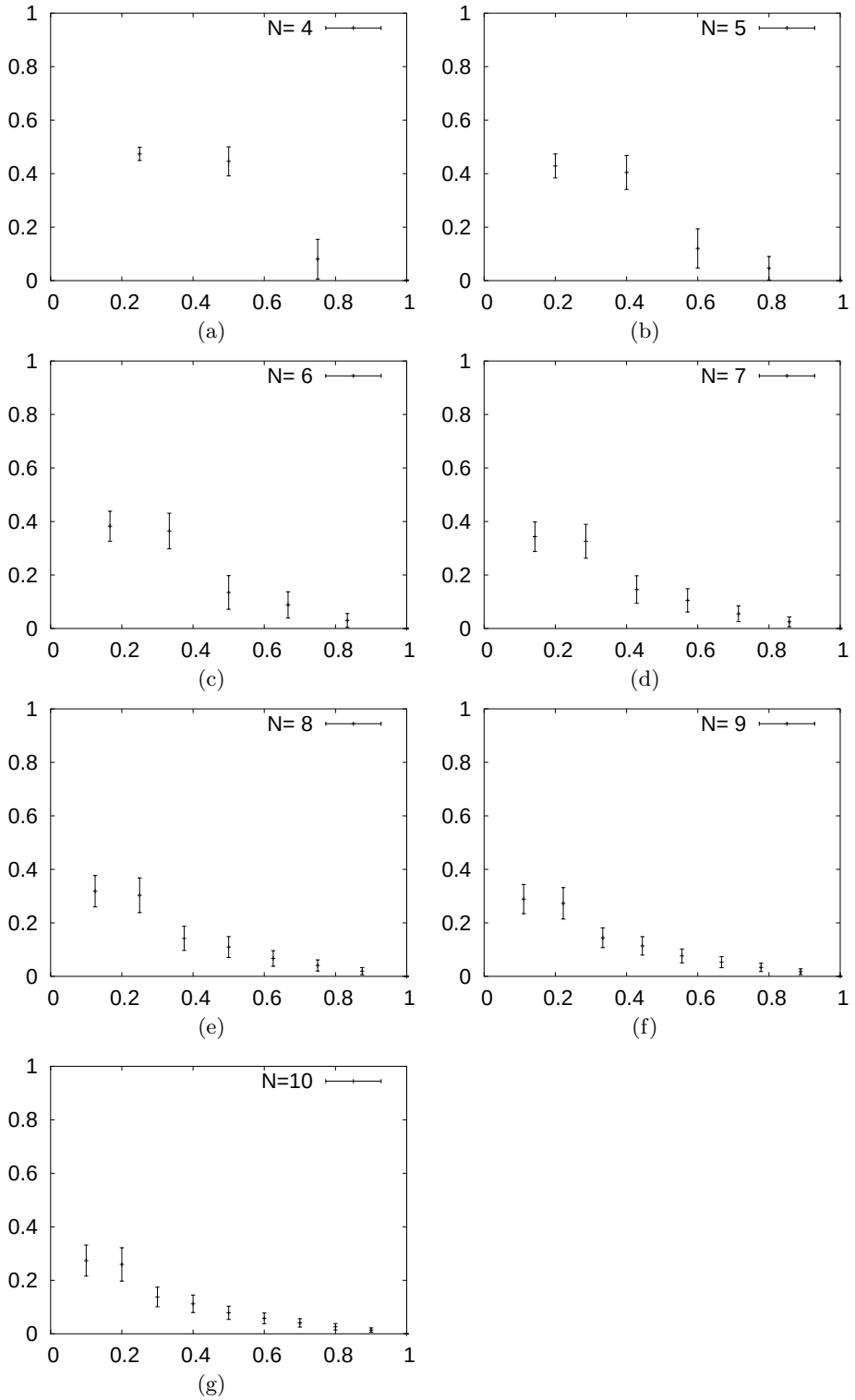

FIGURE 10. Distribution of ensemble averaged normalized singular values, with error bars at one standard deviation about the mean. Note that there appears to be little difference between the distributions shown for $N = 8, 9, 10$.

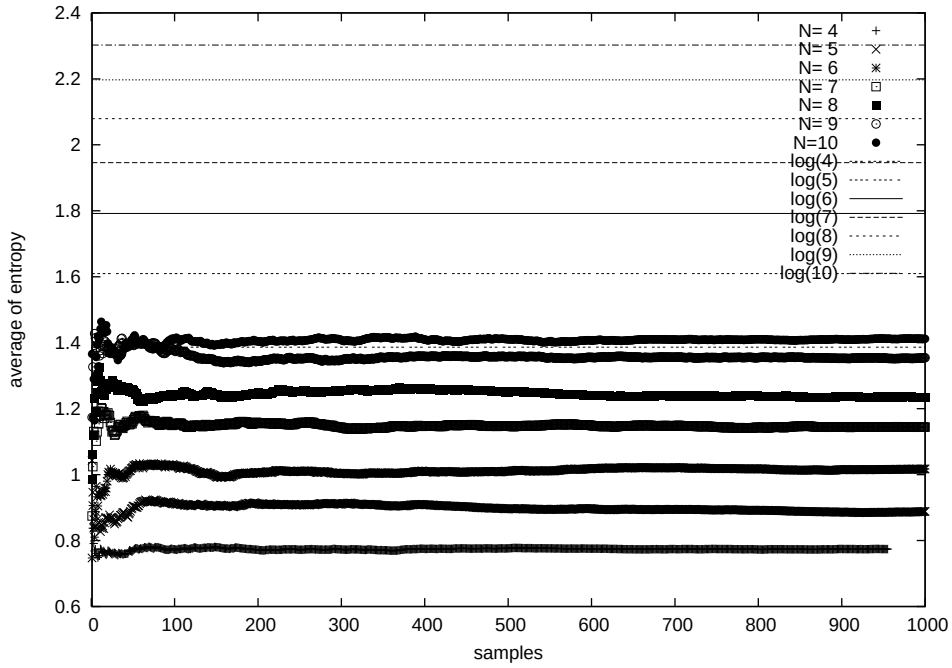

FIGURE 11. Ensemble averaged entropy levels for $N = 4 - 10$, compared with the maximum entropy $\ln(N)$.

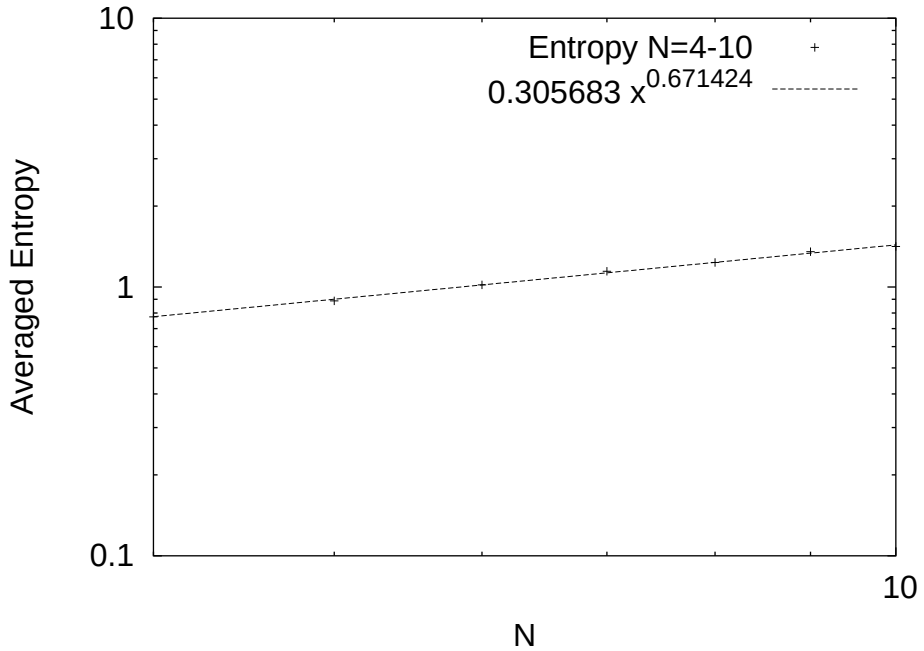

FIGURE 12. Ensemble averaged Shannon entropy values shown in Table 3, plotted as a function of N on a log-log scale. The data shows power-law scaling of the form $< S > \sim \alpha N^{\beta}$, with $\alpha \sim 0.305683$, $\beta \sim 0.671424$ as obtained via a least squares fit to the data.

N	$< S >$	$<< S >>$	$< \|\| \cdot \|\| >$	$<< \|\| \cdot \|\| >>$
4	7.74e-01	9.71e-02	2.75e+00	5.32e+00
5	8.88e-01	1.64e-01	4.78e+00	1.32e+01
6	1.02e+00	2.07e-01	7.96e+00	1.25e+01
7	1.14e+00	2.30e-01	1.04e+01	1.09e+01
8	1.23e+00	2.51e-01	1.63e+01	2.11e+01
9	1.35e+00	2.51e-01	1.89e+01	1.46e+01
10	1.42e+01	2.75e-01	2.75e+01	4.27e+01

TABLE 3. Ensemble averaged Shannon entropy and Frobenius norms with standard deviations for $N = 4 - 10$. Each ensemble consists of 1000 equilibrium configurations.

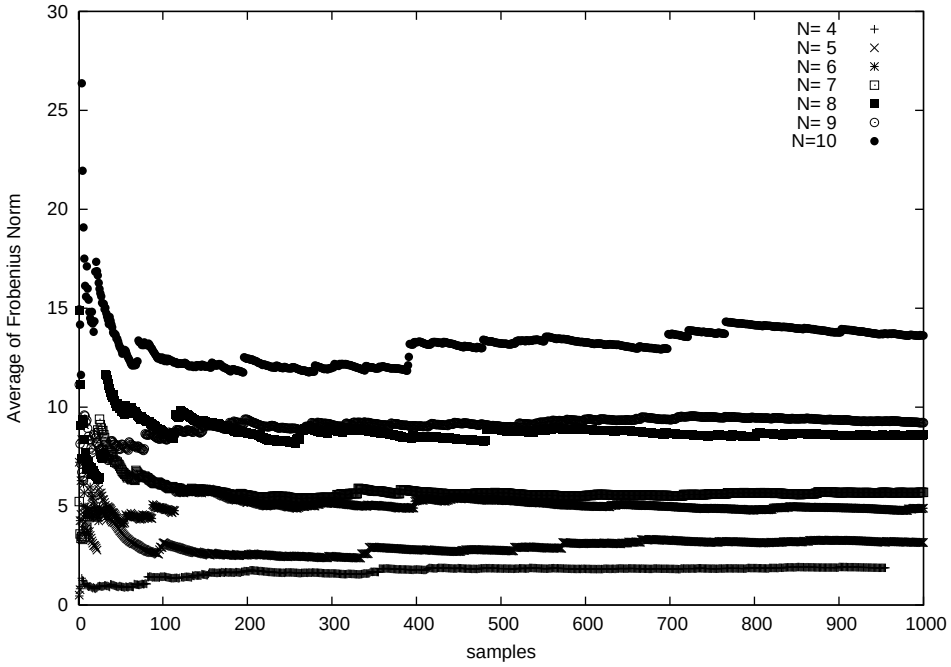

FIGURE 13. Ensemble averaged Frobenius norms for $N = 4 - 10$.

(a) The length of the center-of-vorticity vector, $\|\mathbf{J}\|$ clusters near one, as shown in the histograms of figure 8, while the total vorticity associated with each member of the ensemble, as expressed by $\sum_{i=1}^{N} \Gamma_i^{(j)}$, tends to cluster at the extreme values of ± 1 as shown in the histograms in figure 14.

(b) The averaged Shannon entropy scales very nearly like $< S > \approx \alpha N^{\beta}$, with $\beta \sim 2/3$. This quantity reflects the averaged distribution of the normalized singular values shown in figure 10 as a function of N and provides a scalar measure of the relative weighting of the rank-one components, $\vec{u}_i \vec{v}_i^T$, constituting the equilibrium 'pattern', as encoded in the configuration matrix and expressed in (2.12).

The first conclusion provides evidence that the macroscopic average vorticity can be thought of as one single vortex of unit strength, with either clockwise or counterclockwise circulation, discretized, in a sense, by the point vortices in their relative equilibrium configuration. Since this macroscopic state is in agreement with statistical results reported

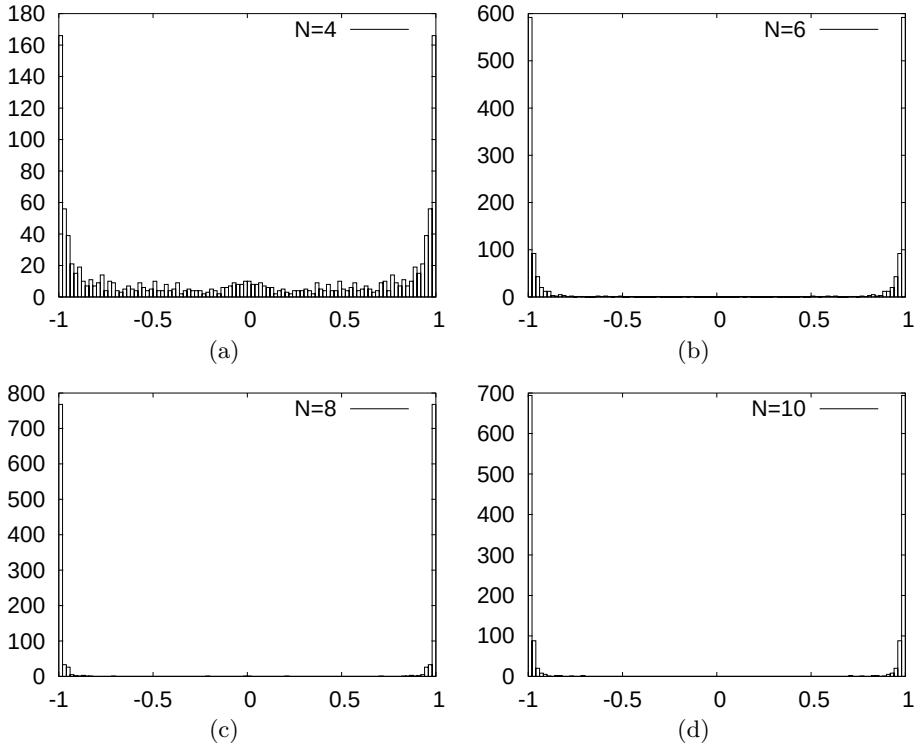

FIGURE 14. Histograms showing the total vortex strength of the ensemble. (a) $N = 4$; (b) $N = 6$; (c) $N = 8$; (d) $N = 10$. Note the tendency for $\sum_{i=1}^{N} \Gamma_i$ to cluster at the extreme values ± 1. The 'pure translation' case $\sum_{i=1}^{N} \Gamma_i = 0$ appears to be quite rare.

by mean-field theory using collections of equal strength vortices moving dynamically on the sphere or via Monte Carlo simulations (see the recent monograph of Lim & Nebus (2006)) it suggests that using the full family of relative equilibria (presumably most of them unstable) offers a useful and rich enough set of microscopic building blocks from which to extract meaningful macroscopic information. The second conclusion, we believe is unexpected as there is no a priori reason for the averaged quantities to follow any clean scaling law. Indeed, as shown in figure 13, the ensemble averaged Frobenius norms do not exhibit clear scaling features. The use of equilibria, in lieu of time-averaging over dynamical trajectories as is usually done, offers distinct computational advantages, not the least of which is the numerical accuracy with which these states can be computed as compared with long-time averages based on simulations of typically chaotic systems. As a final remark, we point out that the methods and conclusions reached in this paper are also relevant in treating the classical problem of optimally distributing N charged electrons on the surface of a conducting sphere, an unsolved problem with a long history (see, as an example, Erber and Hockney (1991)) and listed by Smale (2000) as one of the outstanding mathematical problems for the next century.

REFERENCES

Aref H., P.K. Newton, M.A. Stremler, T. Tokieda, D.L. Vainchtein. 2003 Vortex Crystals. *Advances in Applied Mechanics* **Vol. 39** 1–79.

Bogomolov V.A. 1977 Dynamics of vorticity at a sphere. *Fluid Dyn.* **6**, 863–870.

Bogomolov V.A. 1979 Two dimensional fluid dynamics on a sphere. *Izv. Atmos. Oc. Phys.* **15**(1), 18–22.

Bogomolov V.A. 1985 On the motion of a vortex on a rotating sphere. *Izv. Atmos. Oc. Phys.* **21**(4), 298–302.

Borisov A.V., A.E. Pavlov. 1998 Dynamics and statics of vortices on a plane and a sphere I. *Regular and Chaotic Dynamics* T.3. 1, 28–38.

Borisov A.V., V.G. Lebedev. 1998 Dynamics of three vortices on a plane and a sphere II. *Regular and Chaotic Dynamics* T.3. 99–114.

Brillinger D.R. 1997 A particle migrating randomly on a sphere, *J. Theor. Prob.* **10**(2) 429–443.

Bühler O. 2002 Statistical mechanics of strong and weak point vortices in a cylinder, *Phys. of Fluids* **14**(7) July 2139–2149.

Chavanis P.H, Sommeria J., Robert R. 1996 Statistical mechanics of two-dimensional vortices and collisionless stellar systems, Astrophys. J. 471, 385-399.

Erber T., G.M. Hockney 1991 Equilibrium configurations of N equal charges on a sphere, *J. Phys. A: Math. Gen.* **24** L1369–L1377.

Eyink G., H. Spohn 1993 Negative temperature states and large scale long lived vortices in two-dimensional turbulence, *J. Stat. Phys.* **70** (3-4), 833–886.

Jamaloodeen M.I., P.K. Newton 2006 The N-vortex problem on a rotating sphere: II. Heterogeneous Platonic solid equilibria. *Proc. Roy. Soc. London Ser. A*, **462**, 3277–3299.

Joyce G., D. Montgomery 1973 Negative temperature states for the two-dimensional guiding-centre plasma, *J. Plasma Phys.* **10** 107.

Kendall D.G. 1974 Pole-seeking Brownian motion and bird navigation, *J. Roy. Statist. Soc.* **36B** 365–417.

Kidambi R., P.K. Newton 1998 Motion of three point vortices on a sphere. *Physica D* **116** 143–175.

Kidambi R., P.K. Newton 2000 Streamline topologies for integrable vortex motion on a sphere. *Physica D* **140** 95–125.

Kimura Y., H. Okamoto 1987 Vortex motion on a sphere. *J. Phys. Soc. Japan* **56** 4203–4210.

Kraichnan R., D. Montgomery 1980 Two-dimensional turbulence, *Rep. Prog. Phys.* **43** 547.

Lim C.C., J. Montaldi, M.R. Roberts 2001 Relative equilibria of point vortices on the sphere. *Physica D* **148**, 97–135.

Lim C.C. , J. Nebus 2006 **Vorticity, Statistical Mechanics, and Monte Carlo Simulation**, Springer Monographs in Mathematics, Springer-Verlag, New York.

Lim C.C, J. Nebus, S.M. Assad 2003a Monte-Carlo and polyhedron based simulations I. Extremal states of the logarithmic N-body problem on a sphere. *Discrete and Cont. Dyn. Sys. B* **3(3)**, 213–341.

Lim C.C, J. Nebus, S.M. Assad 2003b A Monte-Carlo algorithm for the free and coaxial extremal states of the vortex N-body problem on a sphere. *Physica A* **328**, 53–96.

Lions P.L., A.J. Majda 2000 Equilibrium statistical theory for nearly parallel vortex filaments, *Comm. Pure Appl. Math.* **8** 76.

Majda A., X. Wang 2006 **Nonlinear Dynamics and Statistical Theories for Basic Geophysical Flows**, Cambridge University Press.

Marcus P.S. 1988 Numerical simulations of Jupiters Great Red Spot. *Nature* **Vol. 331**, 693–393.

Marcus P.S. 1993 Jupiter's Great Red Spot and other vortices. *Ann. Rev. Astron. Astrophys.* **Vol. 31**, 523-573.

Miller J., P.B. Weichman, M.C. Cross 1992 Statistical mechanics, Euler's equation, and Jupiter's Red Spot, *Phys. Rev. A* **45** 4, 2328–2359.

Montgomery D., G. Joyce 1974 Statistical mechanics of 'negative temperature' states, *Phys. of Fluids* **17** 1139.

Newton P.K. 2001 **The N-Vortex Problem: Analytical Techniques**. Applied Math. Sci. **145**, Springer-Verlag, New York.

Newton P.K., G. Chamoun. 2007a Construction of point vortex equilibria via Brownian ratchets, *Proc. Roy. Soc. London Ser. A* **Vol. 463**, 1525–1540.

Newton P.K., G. Chamoun. 2007b Vortex lattice theory: A particle interaction perspective, USC/AME (preprint).

Newton P.K., T. Sakajo. 2007 The N-vortex problem on a rotating sphere: III. Ring configurations coupled to a background field. *Proc. Roy. Soc. London Ser. A* **Vol. 463**, 961–977.

Newton P.K., H. Shokraneh. 2006 The N-vortex problem on a rotating sphere: I. Multi-frequency configurations. *Proc. Roy. Soc. London Ser. A* **Vol. 462**, 2065, 149–169.

Newton P.K., H. Shokraneh. 2007 The N-vortex problem on a rotating sphere: IV. Dipoles as interacting billiards, USC/AME (preprint).

Newton P.K., S.D. Ross 2006 Chaotic advection in the restricted four vortex problem on a sphere, *Physica D* **Vol. 223**, Issue 1, 36–53.

Onsager L. 1949 Statistical hydrodynamics, *Nuovo Cimento Suppl.* **6** 279.

Pointin Y.B., T.S. Lundgren 1976 Statistical mechanics of two-dimensional vortices in a bounded container, *Phys. of Fluids* **19** 1459.

Polvani L.M., D.G. Dritschel. 1993 Wave and vortex dynamics on the surface of a sphere. *J. Fluid Mech.* **255**, 35–64.

Riemann P. 2002 Brownian motors: noisy transport far from equilibrium, *Phys. Reports* **361** 57–265.

Robert R. 1991 A maximum entropy principle for two-dimensional perfect fluid dynamics, *J. Stat. Phys.* **65**(3-4) 531–553.

Robert R., J. Sommeria 1991 Statistical equilibrium states for two dimensional flows, *J. Fluid Mech.* **229** 291–310.

Roberts P.H., H.D. Ursell 1960 Random walk on a sphere and on a Riemannian manifold, *Phil. Trans. Roy. Soc. Lond.* **252A** 317–356.

Sakajo T. 1999 The motion of three point vortices on a sphere, *Japan J. Ind. Appl. Math.* **16** 321–330.

Sakajo T. 2007 Integrable four vortex motion on sphere with zero moment of vorticity, *Phys. of Fluids* **19** 017109-1– 017109-10.

Shannon C.E. 1948 A mathematical theory of communication, Bell. Sys. Tech. J., 27, 379–423.

Smale S. 2000 Mathematical problems for the next century, *Mathematics: Frontiers and Perspectives* 271–294, AMS Providence RI.

Trefethen L.N., D. Bau III 1997 *Numerical Linear Algebra*, SIAM Publishing, Philadelphia.